



Shear resistance of masonry panel in infilled RC frames

Arton D. Dautaj¹ · Ali Muriqi¹ · Cene Krasniqi¹ · Burbuqe Shatri¹

Received: 8 April 2018 / Accepted: 30 March 2019 / Published online: 6 April 2019
© The Author(s) 2019

Abstract

The shear capacity of masonry-infilled reinforced concrete (RC) frames is determined experimentally by testing of five 2/3 scale, one story, one bay infilled RC frame specimens with varying degrees of separation between upper and lower portions of the masonry infill panel. The main premise of this experimental study was to find the contribution of masonry panel in global resistance of infilled RC frames versus shear force. Based on the experimental results, a new method is proposed for the determination of the shear resistance and the contribution of the masonry infill panel is derived. Comparisons of experimental and analytical results show that the proposed method for evaluating the shear resistance of the masonry panels offers a promising approach for the design of infilled RC frames. Furthermore, the results of this study indicate that the shear resistance of masonry panel in infilled RC frames is strongly influenced by the stiffness and lateral resistance of the RC frame.

Keywords Shear resistance · Masonry infill · Bed joints · Frames · Reinforced concrete

Introduction

There have been numerous experimental investigations to determine the shear strength of masonry infill panels. Figure 1 presents some of the test methods that have been previously used to induce shear stresses in masonry infill panels.

As reported by Crisafuli (1997), Baushinger was the first to conduct tests investigating the strength of masonry subjected to shear forces. The simplest such test is the direct shear test on a masonry prism built with a small number of masonry units, as seen in Fig. 1a, b. These specimens both have only one or two layers of mortar, and there is no mortar joint parallel to the compressive load. The test procedures shown in Fig. 1c, d provide more realistic tests because the specimen has a greater number of masonry units as well as mortar layers in two directions as mention

by Morton (2012) and Paulay and Priestley (1992). Having mortar planes in multiple directions is helpful as the shear strength of masonry is known to be dependent on the level of normal stresses in the bed joint of the masonry (Dautaj et al. 2018; Paulay and Priestley 1992; Smith and Carter 1969; Tomazevic 1999).

There are currently two models for the mechanism of masonry shear failure: a friction-based hypothesis and a crack-based hypothesis. The model for determining the shear strength based on friction theory is currently accepted by Eurocode 6 (Crisafuli 1997; Morton 2012; Smith and Carter 1969; Tomazevic 1999; Comite Euro-International Du Beton 1994). According to this model, the shear strength of masonry under shear force is defined as the sum of the shear strength under zero compressive stresses, Eq. (1) and the strength that results from the friction between the mortar and the masonry units, which is dependent on compressive stresses perpendicular to the direction of shear (in the bed joints), Eq. (2). Figure 2 shows the resulting characteristic values of the initial shear strength and the characteristic angle of internal friction, obtained from a shear test conducted on a masonry panel in accordance with EN 1052-3 (2007), for different preloads P :

$$f_v = F/2A, \quad (1)$$

$$\sigma_p = P/A. \quad (2)$$

✉ Ali Muriqi
alishmuriqi@uni-pr.edu

Arton D. Dautaj
arton.dautaj@uni-pr.edu

Cene Krasniqi
cene.krasniqi@uni-pr.edu

Burbuqe Shatri
burbuqe.shatri@uni-pr.edu

¹ Civil Engineering Faculty, Hasan Prishtina University, Pristina, Kosovo



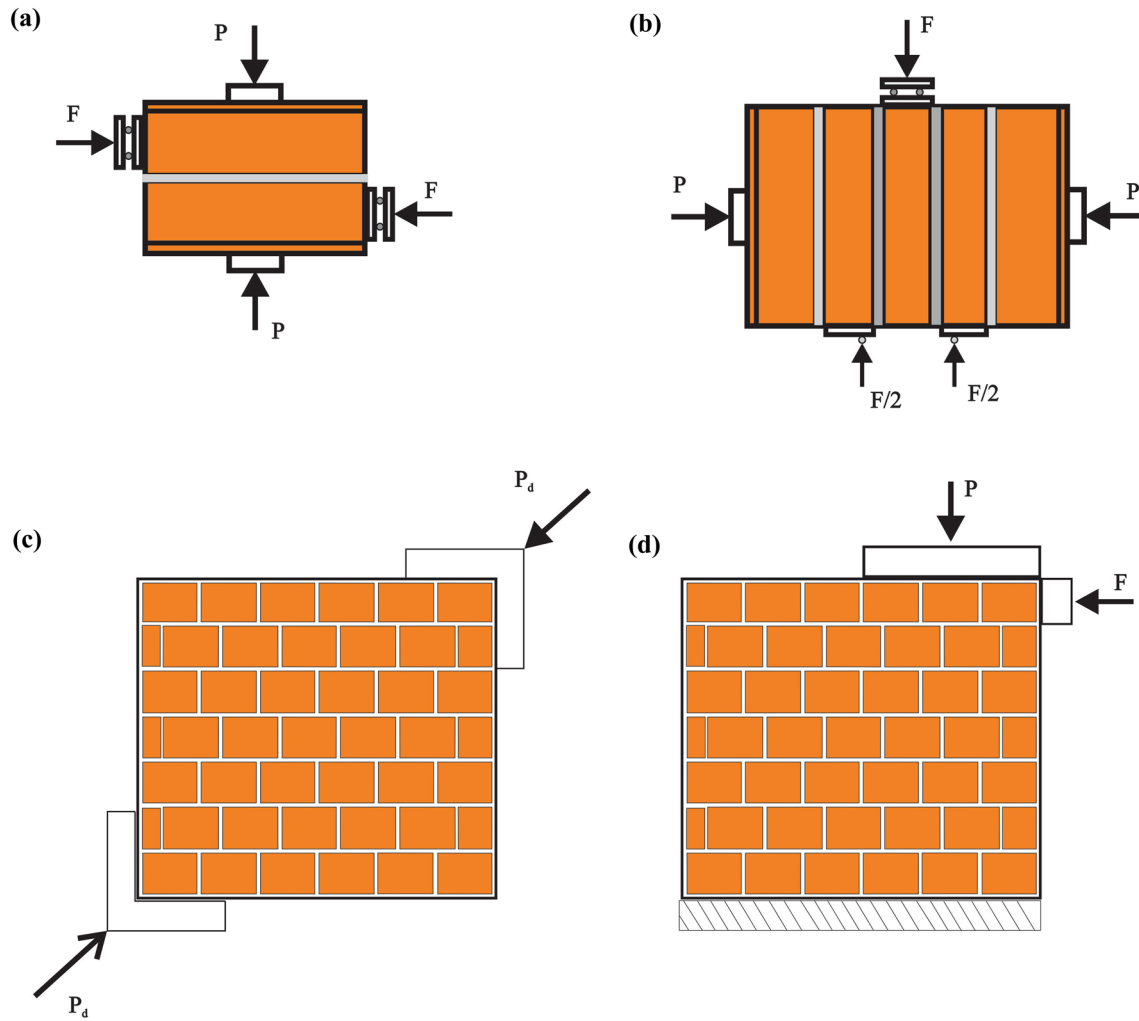


Fig. 1 Different load application methods used in testing of shear strength of masonry infill

Fig. 2 Characteristic values obtained from shear tests according to EN 1052-3 (2007)

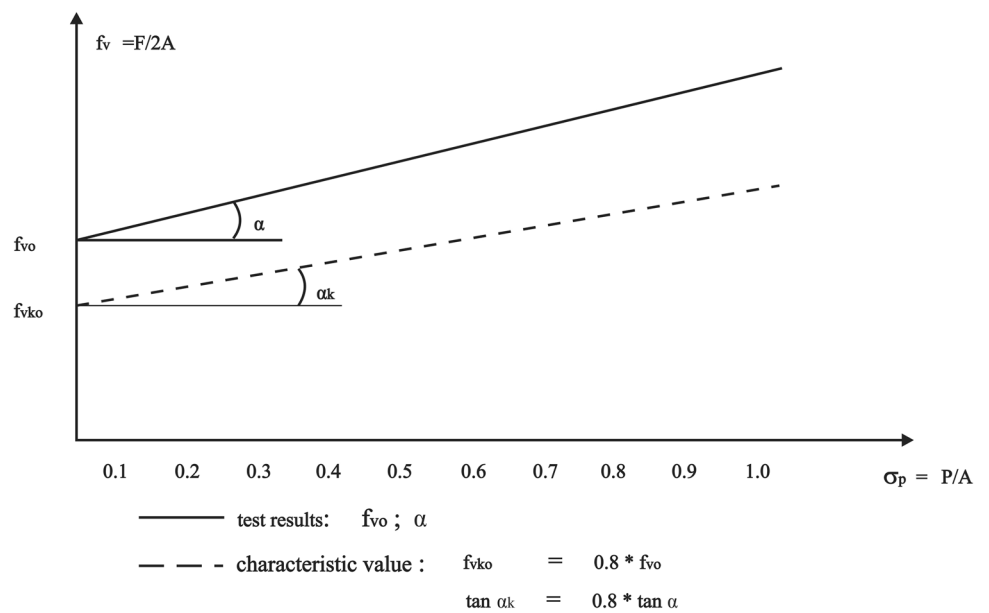


Table 1 Values of f_{vk0} and limiting values of f_{vk} for general purpose mortar

Masonry unit type	Mortar	f_{vk0} (N/mm ²)	f_{vlt} (N/mm ²)
Group 2b clay units	M10–M20	0.3	1.4
	M2.5–M9	0.2	1.2
	M1–M2	0.1	1

The parameters measured in this experiment primarily quantify the behaviour of the bed joints of the masonry. To determine the minimum shear strength of the panel, five such tests must be conducted. Therefore, from the geometry of the test setup and the test results shown in Fig. 2, the basic equation for the characteristic shear strength of unreinforced masonry is given by:

$$f_{vk} = f_{vk0} + 0.4\sigma_d \leq 0.065f_b \tag{3}$$

Table 1 shows the initial shear strength and limit values obtained for the current study in which: σ_d is the design compressive stress perpendicular to the shear, σ_p is the compressive stress perpendicular to the shear, f_{v0} is the shear strength of the masonry units under zero compressive stress, f_{vk0} is the characteristic initial shear strength under zero compressive stress, f_{vk} is the characteristic shear strength of unreinforced masonry not greater than $0.065f_b$ or f_{vlt} , f_{vlt} is a limiting value dictated by the specific national code and, f_b is the normalized compressive strength of the masonry units.

To determine the lateral resistance of masonry failing in shear, the characteristic value of shear strength is multiplied by the resisting cross-sectional area of the wall. For the assessment of seismic resistance according to CEN EC 6 (2004) and CEN EC 8 (2004), the design shear resistance is given by Tomazevic (1999) in Eq. (4):

$$H_{sd,w} = \frac{f_{vk} t l_c}{\gamma_M} \tag{4}$$

where t is the thickness of the wall; l_c is the length of the compressed portion of the wall; and γ_M is the material partial safety factor.

Note that as Eq. (3) represents the shear strength of the mortar and masonry unit interface, it is valid only in those cases in which failure occurs by debonding of mortar joints, meaning that the masonry units must have a greater compressive strength than the mortar. Numerous factors may affect the shear strength between hollow clay blocks and mortar. The most important factors, related to the materials are: blocks and mortar.

Table 2 Evaluation of the shear strength and resistance of masonry panel according to different model

Smith and Carter	Paulay and Priestley	EC8/EC6
$V_w = \frac{f_{v0}}{1.43 - \mu \left(\frac{0.8t_w}{L_m} - 0.2 \right)} L_m t_m$	$V_w = \frac{f_{v0}}{1 - \mu \frac{h_m}{L_m}} L_m t_m$	$V_w = (f_{v0} + \mu 0.4) L_m t_m$

f_{v0} is initial shear strength of bed joints, μ is friction coefficient

Several studies have been conducted to study the influence of mortar to shear strength of masonry. Rahman and Anad (1994) pointed out that the compressive strength of mortar is related to the shear strength.

Dora Foti et al. (2018) also investigated the behaviour of polyurethane foams, used for the construction of thin joints brick masonry walls. They concluded that the foam joints were able to improve the ductility and the energy dissipation of the masonry.

Further, Penava et al. (2016) reported that the interlocking of clay block masonry and mortar joints is also one of the factors that influence the shear resistance of a masonry panel. However, the problem of interlocking is not considered in this paper.

The behaviour of hollow brick walls was observed by Ozsayin et al. (2011), they concluded that the masonry walls strengthened with CFRP sheets enhanced shear strength and deformation capacity. Moreover, they pointed out that the quality of mortar is effective on the compressive and shear strength of infill wall.

An analytical model for predicting the shear strength of fiber reinforced mortars (FRM) masonry walls using the artificial neural network (ANN) approach was proposed by Cascardi et al. (2016). They pointed out that the proposed model is capable for predicting in plane shear strength of masonry panels strengthened by FRM systems.

While most design codes have adopted this expression as a general expression of the shear strength regardless of the mechanism of failure, care should be taken that this criterion remains correctly applied to ensure that a safe assessment of the strength of the masonry wall is conducted.

The second model for masonry shear failure, cited by Tomazevic (1999), assumes that diagonal cracks and shear failure are caused by principal tensile stresses which develop in the wall when it is subjected to a combination of vertical and lateral load.

The expressions for the evaluation of the shear resistance of a masonry panel in an infilled RC frame if sliding shear failure occur are proposed by Paulay and Priestley (1992) and Smith and Carter (1969), CEN EC8/ CEN EC6 (2004/2004), etc., Table 2.

Morandi et al. (2018) and Mohammad Noh et al. (2017) presented a comprehensive review on comparison between experimental and different expression by several authors for evaluation of shear strength and pointed out differences between them. However, no analytical methods are reasonably applicable to different types of infilled frame structures.

Despite plenty of test methods and theories in the literature, there is yet no standard procedure in design or research literature for determining the shear strength of masonry in infilled RC frames.

Due to the complex behaviour of masonry structures in shear and its dependence on many different factors as described at Dautaj et al. (2018) and Razzaghi and Javidnia (2015) the research program discussed in this paper was focused on the following objectives:

- To experimentally determine the shear resistance (which is actually the shear through the mortar) of the masonry panel in an infilled RC frame.
- To propose an analytical method to determine the shear forces resisted by the masonry panel in the infilled RC frames when sliding-mode failure occurs.

To meet these objectives, five specimens were tested and analysed during this research program.

Materials and methods

Test specimens

This research programme involved the testing of five, 2/3 scale, single bay, single story RC frame specimens representing the lower portion of a two-story building. The reinforced concrete frames of specimens 1, 2, and 3 were designed according to the common practice followed in the region, in which masonry is frequently used as a structural system. The RC frames of specimens 10 and 15 were designed with a higher lateral resistance than those of specimens 1, 2, and 3

to demonstrate the effect of increasing the lateral resistance of the RC frame on the shear resistance of the masonry infill.

Table 2 and Fig. 3 provide the geometries and steel reinforcement details of the specimens. Specimen 1 is a bare frame, while specimens 2 and 10 were infilled with hollow clay blocks containing no separation (split) in the middle of the masonry panel. In specimen 3, the bed joint in the middle of the masonry panel was eliminated with a separation to ensure that the horizontal shear force across the middle of the panel was zero. In specimen 15, the bed joint was partially developed so the horizontal shear force would only be present in the middle of the panel. This distance likely encompasses the limits of the horizontal component of the diagonal strut, as shown in Fig. 3.

Masonry units of similar size and material were used to construct the masonry infill for all specimens. The masonry infill units used were hollow clay blocks with holes consisting of about 65.8% of the total block volume, as shown in Fig. 3b.

The construction of the test specimens began by preparing the reinforcement cages for the foundation beam, the columns, and the top beam. Then, forms were constructed for the foundation and concrete was cast, followed by formwork and casting of the columns and beams. The masonry walls were constructed after the formwork was removed from the frame (after 28 days curing time), as per the most common method for infilled RC-frame construction.

Material properties

Material properties were evaluated using the relevant standards by conducting tests on the masonry units, mortar, concrete, and reinforcing bars (Table 3). The normalized compressive strength of the masonry units

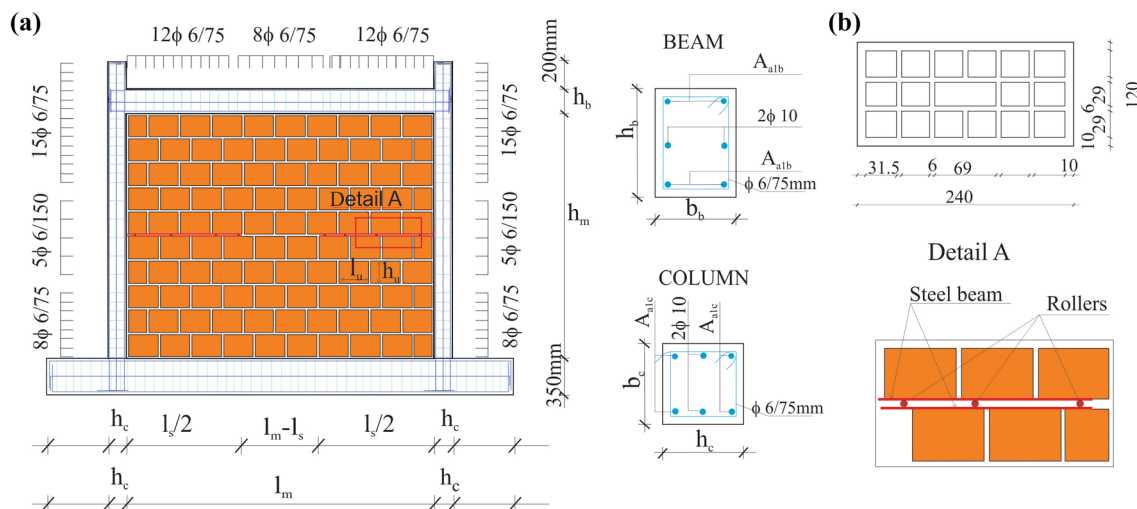


Fig. 3 a General geometry of test specimens, b hollow clay block (unit: mm)



Table 3 Dimensions and material properties of the test specimens

Specimen property	Specimen				
	1	2	3	10	15
f_y —yield strength of reinforcement (N/mm ²)	620	620	620	620	620
h_c —height of columns (mm)	150	150	150	250	200
b_c —width of columns (mm)	150	150	150	150	150
h_b —height of beam (mm)	200	200	200	250	200
b_b —width of beam (mm)	150	150	150	150	150
l_m —length of masonry panel (mm)	–	2500	2500	2300	2400
h_m —height of masonry panel (mm)	–	2000	2000	1950	1000
l_s —split length in the middle of masonry panel (mm)	–	0	2500	0	1500
A_{a1c} —area of tension and compression reinforcement for columns (mm ²)	157	157	157	157	234
A_{a1b} —area of tension and compression reinforcement for beam (mm ²)	157	157	157	157	234
h_u —height of masonry units (mm)	–	200	200	200	200
l_u —length of masonry units (mm)	–	250	250	250	250
t —thickness of masonry units (mm)	–	120	120	120	120
f_m —mean compressive strength of mortar (N/mm ²)	–	9.75	12.03	9.75	11.87
f_{tm} —flexural strength of mortar (N/mm ²)	–	3.2	2.34	2.34	3.69
$f_{b,p}$ —normalised compressive strength of masonry units parallel to holes (N/mm ²)	–	14.38	14.38	14.8	14.38
$f_{k,p}$ —characteristic compressive strength of masonry parallel to holes (N/mm ²)	–	3.99	3.99	3.99	3.99
$f_{b,o}$ —normalised compressive strength of masonry units orthogonal to holes (N/mm ²)	–	5.11	4.21	5.11	5.17
$f_{k,o}$ —characteristic compressive strength of masonry orthogonal to holes (N/mm ²)	–	2.04	2.15	2.04	2.64
f_c —compressive strength of the concrete (N/mm ²)	25	24.5	24.5	25	24

used was determined according to CEN EC 6 (2004) and EN 772-1 (2011), and the results are presented in Table 2. The mortar used in these tests was produced according to predetermined constituent mix proportions, e.g., 1:0.25–0.5:2.25–3 of cement:lime:sand by volume, and the expected mean value of its compressive strength was 10 MPa (Mortar type-M10). The bending and compression testing of these mortars was conducted according to the EN 1015-11 (2007) and EN 12190 (2000) requirements, respectively. The characteristic compressive strength of the masonry was determined based on CEN EC 6 (2004) and Soric (2000). The compressive strength of the concrete was obtained according to EN 12390-3 (2002) by testing a 150 × 150 × 150 mm cube.

In all, 26 compression tests were performed on the masonry units, 15 compression tests on the concrete, 50 compression tests and 25 flexural tests on the mortar, and 30 tensile tests on the reinforcement, with the results shown in Table 3.

The lateral resistances of the bare frames of specimens 1, 2, 3, 10, and 15 were evaluated according to pushover analysis. The lateral resistances of the bare frames, given by P^i , where i is the specimen number, were found to be about $P_{fr}^{15} = 42$ kN, $P_{fr}^{10} = 52.5$ kN, and $P_{fr}^{1,2,3} = 24.5$ kN, Fig. 4.

Test set-up and procedure

Figure 5 shows the testing apparatus used in this study. The apparatus includes a steel reaction frame, a loading system, and an instrumentation system. The steel reaction or loading frame comprised two HE section columns that were connected at the top and bottom by two beams, as well as a blocking mechanism that limited horizontal and vertical displacement and out-of-plane displacement at the bottom and top of the specimen, respectively.

The loading system, controlled using a multi-functional console, comprised two horizontal and one vertical hydraulic actuators operated by a hydraulic pump and actuator control software. The two horizontal hydraulic actuators had a load capacity of 300 kN (± 100 mm stroke) and were used in conjunction to push or pull the top beam of the masonry-infilled RC frame located 2.4 m above the bottom beam of the reaction frame. The vertical hydraulic actuator had a load capacity of 200 kN (± 100 mm stroke) and was used to apply a concentric vertical load to the frame columns via load distribution beams.

The instrumentation system included three load cells, which are located in the each actuator arm, each with a maximum load capacity of 200–500 kN. The instrumentation system also included six displacement transducers



Fig. 4 Pushover curve of bare frame for selected specimens

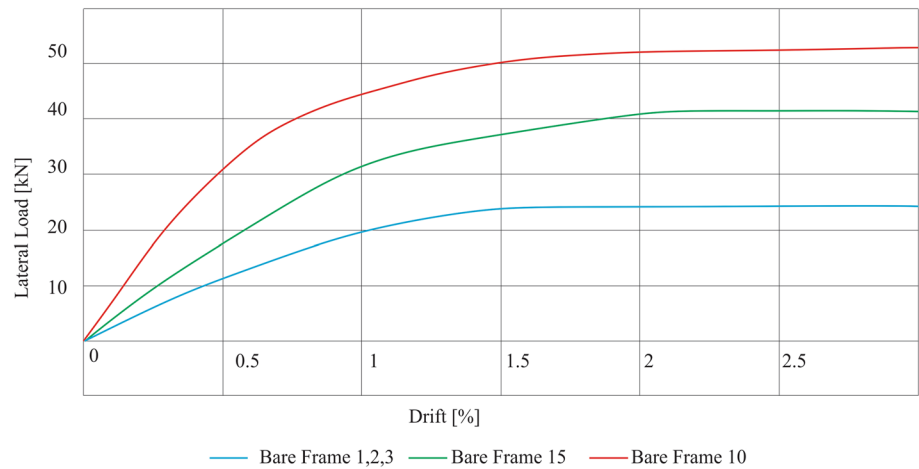
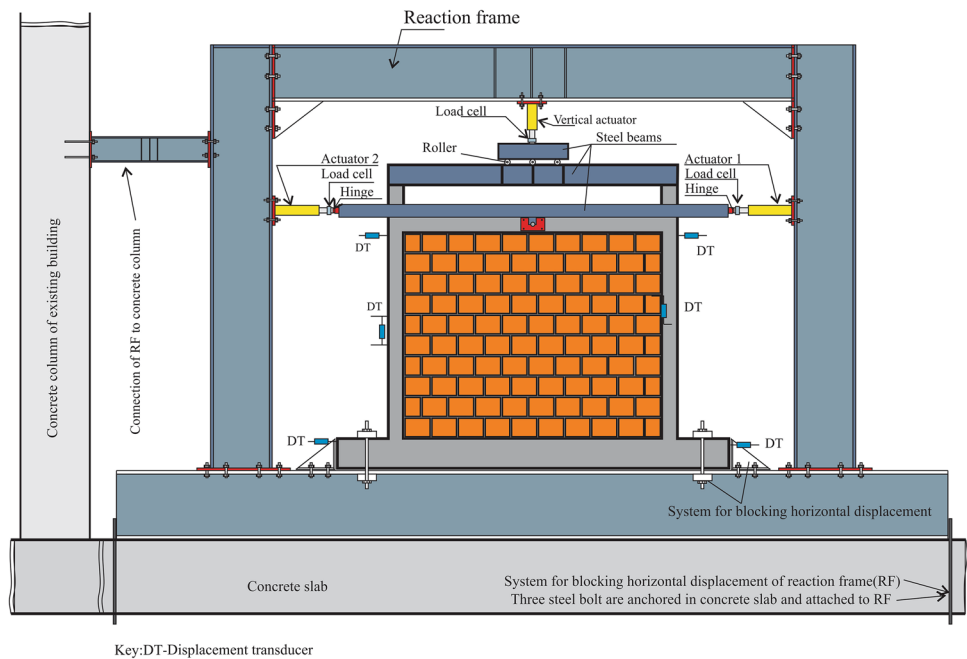


Fig. 5 Loading frame and instruments used in the test



with accuracies of $> \pm 0.1\%$ and $> \pm 0.2\%$ for ranges of up to 25 and 100 mm, respectively. Two transducers (± 100 mm stroke), positioned on the top beam of the specimen 2.2 m from the bottom beam of the reaction frame, were used to measure the horizontal displacement of the specimen. The third transducer (± 100 mm stroke), positioned 1.5 m from the bottom beam of the specimen, was used to measure the separation between the masonry panel and the RC frame. The fourth transducer (± 100 mm stroke) was used to measure the displacement at the middle of the RC frame column. The remaining two transducers (± 50 mm stroke) were used to measure the horizontal displacement at the base of the specimen.

Initially the specimens were loaded and unloaded with a small proof load to confirm the effectiveness of instrument

set-up and loading. Most of the specimens were subjected to quasi-static cyclic loads in both directions, only specimen 15 was subjected to monotonic loading in one direction. Five to ten cycles in each direction were applied with a load increment between each cycle of 10 kN. To simulate gravity loads from upper stories, a constant vertical force of 20 kN (estimated as the total weight of a two-story building, concentrated at the floor level and distributed equally to the columns) was applied at the top of each column. Data measured from the load cells and displacement transducers was stored using the data logger unit, and computer software was used to read the force and displacements in real time.



Test results

Experimental results

Specimen 1

For specimen 1, which is bare frame, the first crack occurred in the bottom and top of column when lateral displacement was 8 mm. At lateral load $P_y=22$ kN, specimen 1 started yielding for corresponding displacement $\Delta y=40$ mm (drift ratio 2.0%). Beyond this point, the bare frame showed the change in behaviour and stiffness degradation up to maximum lateral load which was $P_{\max}^1=24.5$ kN, which is approximately the same as the predicted lateral strength resulting from a “pushover analysis”. It can be noticed that the bare frame exhibited ductile behaviour, with displacement ductility at about 5.1, Fig. 6. Specimen 1. This specimen was tested to serve as a comparison for the behaviours of the masonry-infilled specimens.

Specimen 2

Specimen 2 was subjected to cyclic load for total five cycles in two direction and two cycles in one direction. During

testing, an initial stepped crack induced by shear forces in the masonry occurred during cycle 4 under a force level of 45–56 kN and a corresponding displacement of $d=6$ mm (a drift ratio of 0.3%). During this same loading cycle, cracks also occurred in the left beam–column joint and in the middle of the left column.

When the lateral load was increased towards the right during cycle 5, additional cracks formed in the masonry, beam–column joint, and column. The maximum lateral force resisted by Unit 2 (P_{\max}^2) was observed during cycle 5. During this cycle, $P_{\max}^2=94.17$ kN and its associated displacement (d) was $d=40$ mm (a drift ratio of 2.0%). The lower part of the left column remained vertical. The highest flexural deformation was instead concentrated at the middle of the column, where a plastic hinge formed as a result of the interaction between the lower part of the masonry and the beam–column joint.

The ultimate failure mechanism for specimen 2 was a combination of the masonry infill’s shear failure and plastic hinge formations in the middle of the left column and in the upper and lower parts of the right column. Figure 7 depicts specimen 2’s behaviour during and following testing.

Fig. 6 **a** Cracking at lower and upper parts of the left column, **b** lateral force–displacement response of specimen 1, Dautaj et al. (2018)

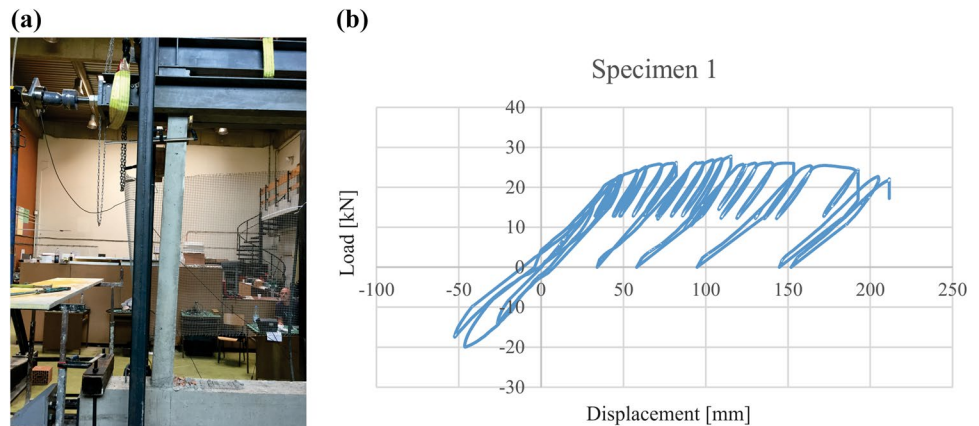


Fig. 7 Specimen 2, **a** details of the beam-to-column joints, **b** cracking of specimen 2 after test, and **c** lateral force–displacement response, Dautaj et al. (2018)

Specimen 3

Specimen 3, which contained a debonded separation in the masonry panel at mid-height, was subjected to a total of four cycles in both directions and three cycles in the left direction, with an applied displacement in excess of 200 mm. As a result of this displacement, there was significant damage to the RC frame, but the masonry infill showed only small cracks. The first cracks in the columns appeared in cycle 3 during the action of the left actuator 2 at a force of $P_{crac}^2 = 35.66$ kN and a corresponding displacement of $d = 10.4$ mm (a drift ratio of 0.52%). In cycle 4, cracks were noted in the left column beam node, and cracks that had formed earlier continued to propagate. Cracks also appeared on the right column, although the focus of this study was on the left column because of the readily forming cracks and plastic hinges observed in its mid-height region. In this cycle, the maximum load of $P_{max}^3 = 53.93$ kN was achieved with a corresponding displacement of $d = 44$ mm (a drift ratio of 2.2%). After the maximum load, the performance of specimen 3 steadily degraded with increasing deformation, decreasing stiffness, and decreasing resistance of the frame. Figure 8 shows the final failure mechanism that occurred during cycle 6 at a displacement of 150 mm. The failure of specimen 3 clearly occurs as a result of the failure of the RC frame, not the masonry infill.

Fig. 8 Specimen 3, **a** ultimate failure mechanism, **b** lateral force–displacement response for all cycles

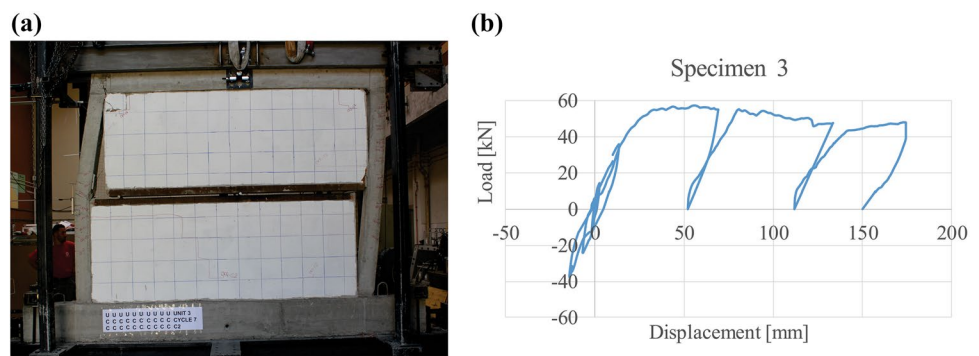
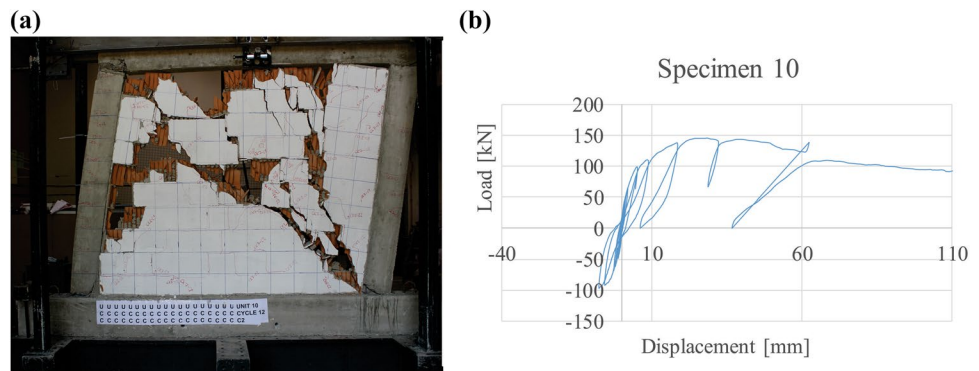


Fig. 9 Specimen 10, **a** ultimate failure mechanism, and **b** lateral force–displacement response for all cycles, Dautaj et al. (2018)



Specimen 10

Specimen 10 was designed to exhibit a greater bare frame lateral resistance compared to that of specimens 2, 3, and 15 by increasing the flexural strength of the columns.

The impact of these changes on the lateral strength of the frame can be noted in the cracking load, maximum resistance of the specimen, as well as in the final failure mechanisms observed. The first crack in specimen 10 appears during cycle 6 while actuator 2 is active at a load of $P_{crac}^{10} = 96.8$ kN, and a corresponding displacement of $d = 4.8$ mm (a drift ratio of 0.24%).

The maximum lateral load resisted by specimen 10 was $P_{max}^{10} = 145$ kN, with a corresponding displacement of $d = 29.5$ mm (a drift ratio of 1.475%), which is greater than the maximum loads resisted by specimens 2 ($P_{max}^2 = 94.6$ kN). It can also be seen from the load–displacement curve of specimen 10, shown in Fig. 9b, that the initial stiffness of specimen 10 was greater than that of specimen 2. The final failure mechanism of specimen 10 (see Fig. 9a) differs from the final mechanism observed in specimen 2 in that after the masonry degraded, plastic hinges developed in discreet locations at the top and bottom of the columns, rather than in the middle of the columns.

Specimen 15

Specimen 15 was subjected to a total of seven load–unloading cycles in the left direction from actuator 2. This specimen was designed to quantify the contribution of the masonry infill panel to the shear resistance of the RC frame when compared to that of a continuous panel (as provided in specimen 2) and a fully split panel (as provided in specimen 3). In addition to the standard displacements common to the other specimens, displacements were also measured just below the location of the panel separation. The first crack appeared in cycle 4 at a load level of $P_{crac}^{15} = 30.5$ kN and a corresponding deformation of $d = 1.55$ mm (a drift ratio of 0.0775%). The first four cycles, and the first crack in specimen 15, are shown in Fig. 10.

In cycle 5, specimen 15 reached a maximum resistance of $P_{max}^{15} = 100.00$ kN with a corresponding displacement of $d = 7.4$ mm (a drift ratio of 0.37%) in the middle of the panel and $d = 19.5$ mm (a drift ratio of 0.975%) at the top beam. In this cycle, the masonry panel sheared into two parts and the RC unit began to degrade. As seen in the force–displacement diagram of Fig. 11, in the middle of the masonry panel, the shear strength was sufficient to resist the load until it had displaced 20 mm, after which the shear resistance decreased.

It can be clearly seen that the destruction of specimen 15 occurred as a result of the shearing of the infilled panel into two parts, which resulted in the formation of hinges in the reinforced concrete frame, effectively creating a frame consisting of two independent diagonals at the top and bottom of the frame (a knee-braced frame).

Proposed method for evaluation of the shear strength of a masonry panel in an infilled frame

Model description

The shear resistance obtained according to the following method is used in the proposed model to estimate lateral strength of masonry-infilled RC frames. Further details and description of the model can be found in Dautaj and Kabashi (2019). In the proposed model, the masonry infill is represented by two diagonal struts and one horizontal tie, Fig. 12b.

For specimen 2 the shear force on masonry panel is determined experimentally $V_f = 45\text{--}56$ kN. Using this force, the forces in diagonal struts 1 and 2 were calculated as follows:

$$S_1 = 1.25 \cdot V_f, \tag{5}$$

$$S_2 = 1.25 \cdot V_f. \tag{6}$$

Fig. 10 Specimen 15, **a** the first crack in the masonry at cycle 4, **b** the force–displacement relationship at the middle of the masonry and at the top beam level

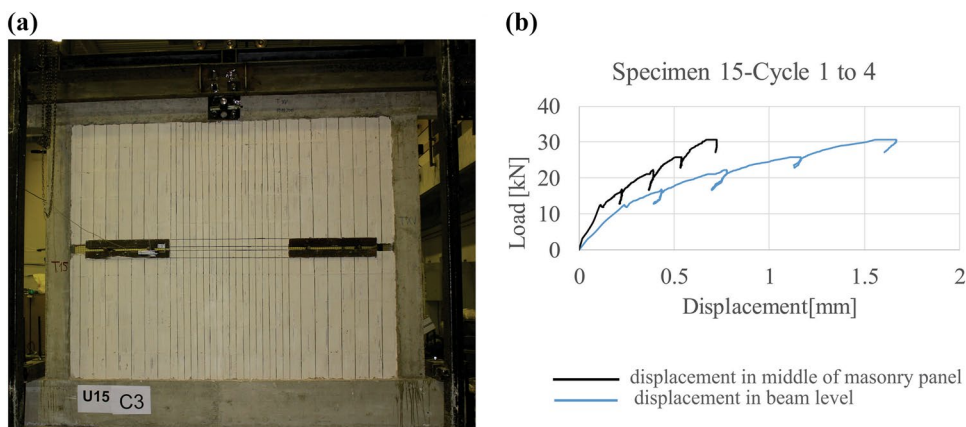
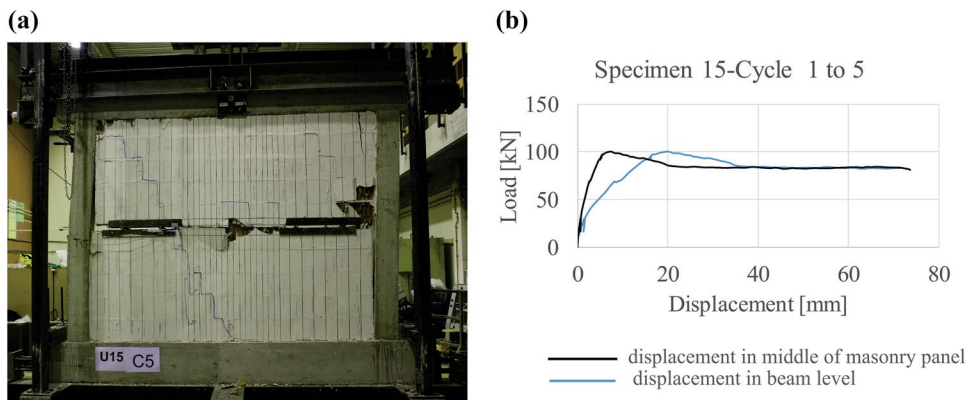


Fig. 11 Specimen 15, **a** sliding shear failure, **b** force–displacement relationship in the middle of masonry panel and top beam level up to 70 mm displacement



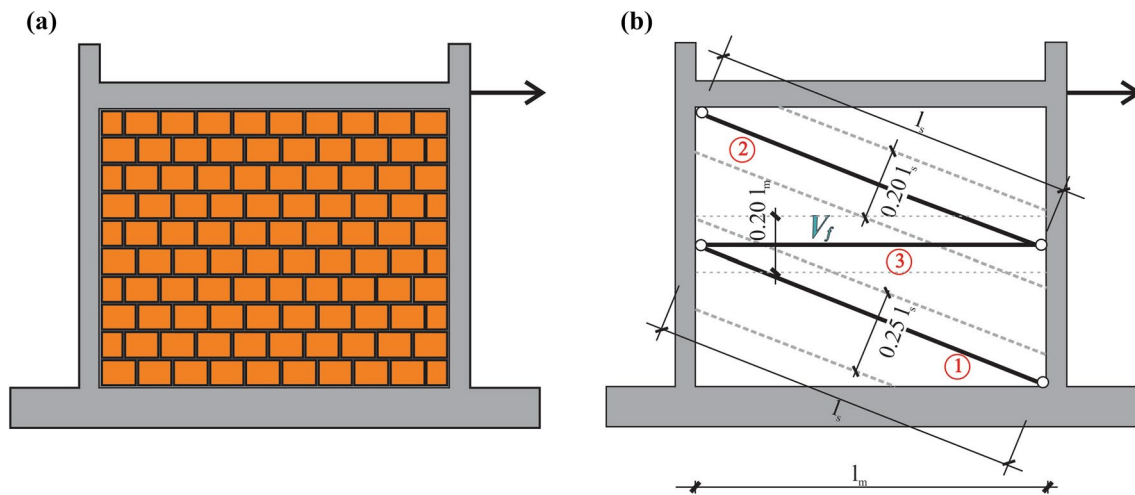


Fig. 12 **a** Masonry-infilled RC frame with hollow blocks, **b** proposed model to analyse the infilled frame, Dautaj and Kabashi (2019)

These relationships were calibrated in the proposed model by setting the observed behaviour of specimen 2 equal to the forces in the struts.

The shear resistance of the masonry infill in the other specimens is given by the shear force function derived for specimen 2, Eq. (7). An increase or decrease in the interaction between the masonry panel and the RC frame reflects a respective increase or decrease in the shear strength of the masonry panel, as demonstrated by this research programme. A greater lateral strength of the bare frame leads to a larger shear force as a results of larger normal forces at the bed joint. Thus:

$$V_{f,i} = 0.9 \frac{V_{y,i}}{V_{y,ek}} V_{f,ek}, \quad (7)$$

where $V_f = V_{f,ek} = V_{f,2} = 45\text{--}56$ kN is the shear resistance (the shear force that initiates a sliding shear failure) that was experimentally determined by the specimen 2 reference test. Analytically, the shear resistance of the masonry infill in specimen 2 was determined as a function of the length of the masonry infill, the thickness of the infill panel, and the initial characteristics of the shear strength under zero compressive stress, such that:

$$V_{f,ek} \leq c \cdot t \cdot l \cdot f_{vk0}, \quad (8)$$

where t is the thickness of the masonry infill; f_{vk0} is the initial characteristic shear strength under zero compressive stress; l is the length of the masonry panel; c is an experimentally determined coefficient (for the reviewed case, $c = 0.56\text{--}0.62$); $V_{y,ek} = V_{y,2}$ is the yield strength of the bare RC frame without masonry infill for specimen 2; $V_{y,i}$ is the yield strength of the bare RC frame without masonry infill for the analysed specimen; and $V_{f,i}$ is the shear resistance

of the masonry infill in the analysed masonry-infilled RC frame.

Note that the force $V_{f,i}$ must satisfy the following requirements: $V_{f,i} \leq l \cdot t \cdot f_{vk}$ and $V_{f,i} \leq w_3 \cdot t \cdot f_k$ (whichever is smaller), where f_{vk} is the characteristic shear strength of the unreinforced masonry, and f_k is the characteristic compressive strength of the masonry.

Analytic results

The shear resistance of the masonry panel in the other specimens is given by Eq. (7) as a function of the measured specimen 2 shear force.

The shear force in strut 3 for specimen 10, calculated from Eq. (7), is $V_{f,10} = 90$ kN, whereas the force in struts 1 and 2 is 113.0 kN. The increase in strength $V_{f,i}$ from 45–56 to 90 kN is due to the increase of normal force across the bed joint for a larger bare RC frame strength.

In same way, the shear resistance of the masonry infill of specimen 15 can be calculated by Eq. (7), as follows:

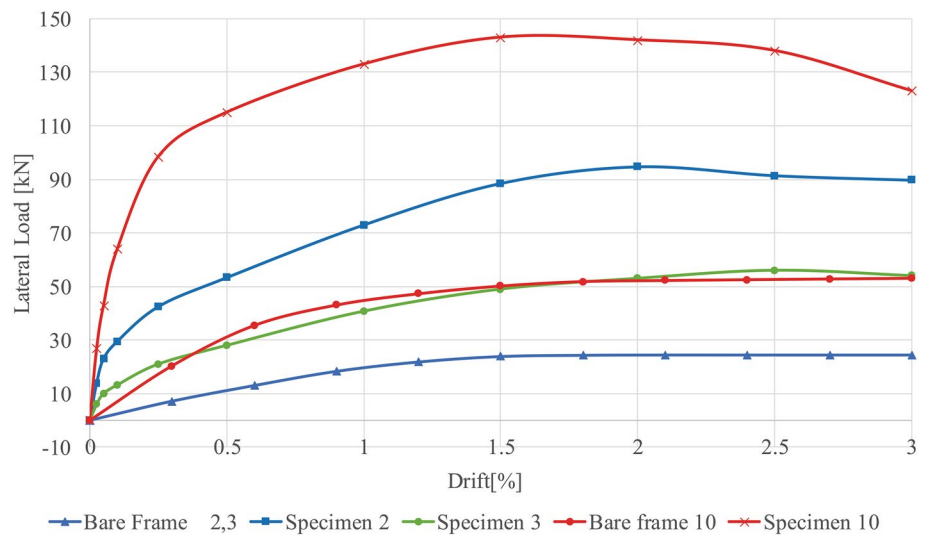
$$V_{f,15} \leq 0.9 \cdot \frac{l_m - l_s}{l_m} \cdot \frac{V_{y,15}}{V_{y,ek}} V_{f,ek} = 0.9 \cdot \frac{90}{240} \cdot \frac{39.1}{23} \cdot 52 = 29.83 \text{ kN}.$$

The obtained shear resistance is used as input data into the above model to analyse the behaviour of the masonry-infilled RC frame.

Comparison of results

In this section, the results of the specimen tests are presented and analysed for characteristic behaviour by comparing their applied load at first cracking, maximum load resisted, and corresponding deformations.

Fig. 13 Load-story drift envelopes of specimens 2, 3 and 10 and Bare Frame 2, 3, 10



These results are compared with the analytical results obtained using the method proposed in “[Model description](#)” for determining the shear resistance of the masonry panel in an RC frame.

Comparing the specimens in question, specimen 3, the masonry-infilled RC frame with masonry infill of no shear resistance in the middle of panel, resisted a maximal lateral load of $P_{max}^3 = 53.93$ kN. When compared to specimen 2, which resisted a maximum lateral load of $P_{max}^2 = 94.17$ kN, it can be seen that the shear resistance of the masonry infill in an RC frame demonstrably increases the lateral shear resistance with a contribution to the general shear resistance of approximately 45–56 kN. This force is about equal to the force at first cracking.

The first crack in specimen 10 appeared at a load of $P_{crac}^{10} = 96.8$ kN and a corresponding displacement of $d = 4.8$ mm. When compared to the capacity obtained by Eq. (7), which was 90 kN, it can be stated that the two values are nearly equal. By comparing the lateral force of specimen 2 with specimen 10 at drift ratio 0.25–0.3%

it can be seen differences between them as a results of the differences in their lateral strength of bare frame 1 and 10, see Fig. 13. The first crack in specimen 15 appeared in cycle 4 at a load of $P_{crac}^{15} = 30.5$ kN and a corresponding deformation of $d_{cr} = 1.55$ mm. When compared with the shear capacity obtained analytically (29.83 kN), these values are clearly nearly equal.

Taking a model A as a test case with similar geometry to that of specimen 15 but with no shear resistance in the middle of masonry infill, according to the model proposed in “[Model description](#)”, it can be demonstrated that lateral resistance of model A at a displacement of 20 mm is 70 kN and its maximum lateral resistance is $M_{d=40mm}^A = 82$ kN. When compared to specimen 15, as shown in Fig. 14, it can be seen that the shear resistance of the masonry infill in an RC frame increases the lateral resistance of the frame, making a noticeable contribution to the general shear resistance of the masonry-infilled RC frame of approximately 26–32 kN.

Fig. 14 Envelope of responses for specimen 15, model A, and bare frame of specimen 15

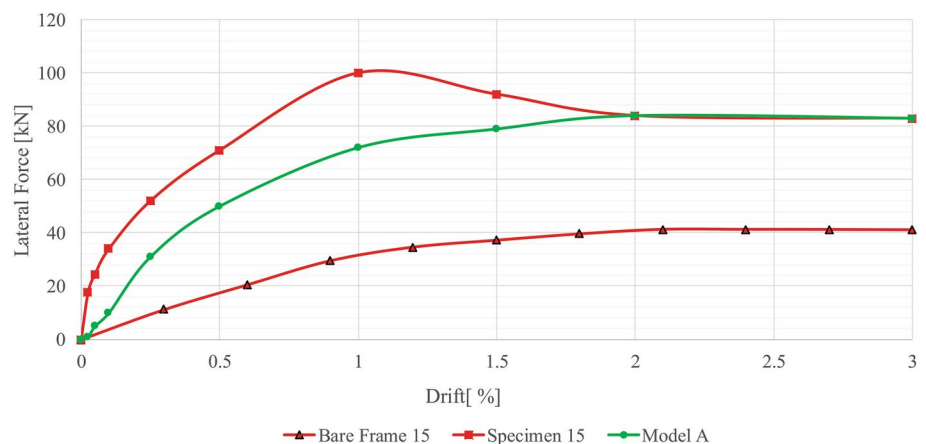


Table 4 Influencing parameters of tested specimens

	P_{cr} (kN)	d_{cr} (%)	P_{max} (kN)	d_{max} (%)	K_s (kN/mm)	K_{fr} (kN/mm)	K_s/K_{fr}	P_{fr} (kN)	$P_{fr}/V_{f,ek}$	P_{max}/P_{fr}
Specimen 1	–	–	24.5	2.2	0.6	0.6	1.0	24.5	–	1.0
Specimen 2	54	0.3	94.2	1.9	2.5	0.6	4.3	24.5	0.5	3.8
Specimen 3	–	–	53.9	2.2	1.2	0.6	2.2	24.5	0.5	2.2
Bare frame 10	–	–	52.5	1.5	1.8	1.8	1.0	52.5	1.0	1.0
Specimen 10	96.8	0.24	145.0	1.5	4.9	1.8	2.8	52.5	1.0	2.8
Bare frame 15	–	–	42.0	1.4	1.5	1.5	1.0	42.0	0.8	1.0
Specimen 15	30.5	0.0775	100.0	1.0	5.0	1.5	3.3	42.0	0.8	2.4

P_{cr} is force that initiates the cracking of the masonry (sliding/diagonal), K_s and K_{fr} is stiffness at maximum load

Table 5 Experimental/analytical shear force comparison

P_{cr} (kN)	Experimental	Paulay and Priestley	Smith and Carter	EC8/EC6	Proposed method
Specimen 2	45–56	210	90	45	52
Specimen 10	96.8	210	90	45	90
Specimen 15	30.5	78.8	33.8	16.8	29.8

P_{cr} is force that initiates cracking of the masonry panel

All tested specimens, the lateral load-and-drift ratio at a characteristic point, the force at first cracking, ratio of bare frame to shear resistance of masonry panel, the ratio between the infilled frame and bare frame stiffness, and the maximum lateral resistance ratio of the infilled frame and bare frame are shown in Table 4.

Furthermore, the shear force in the masonry panels of specimens 2, 10, and 15, were evaluated according to the equations proposed by Paulay and Priestley (1992), Smith and Carter (1969) and CEN EC8 (2004), leading to shear forces that were different from values measured during the experimental tests, and also different from shear forces determined using the proposed method. The expressions proposed by Paulay and Priestley (1992) overestimate shear strength for all units, whereas the strength according to Smith and Carter (1969) is in good agreement with experimental tests for specimen 2 and 15 but leads to overestimate to the shear strength of specimen 2. EC 8 leads to underestimate shear force (fairly good safe results) in comparison with experimental results when one half of f_{v0} is assumed. A similar differences between experimental and proposed expression for shear strength was reported by Morandi et al. (2018). Table 5 presents and compares the shear forces determined experimentally, by the proposed method, and using methods proposed in the literature by different authors.

Conclusions

The main objectives of this experimental study were:

- To experimentally determine the shear resistance (which is actually the shear through the mortar) of the masonry panel in infilled RC frames.
- To propose an analytic method for determining the shear force (the force that initiates sliding) resisted by the masonry panel in infilled RC frames when a sliding-mode failure occurs.

Based on the experimental results, the following conclusions can be drawn.

- Based on the comparison of experimental results, it was observed that the shear strength of masonry panel is influenced by lateral strength of bare frame at low levels of drift ratio (by comparing results between specimens 2 and 10 at drift ratio 0.25–0.3%, which had different lateral resistance of bare frame).
- A comparison of experimental and analytical results demonstrated that the shear resistance of the masonry panel in an infilled RC frame can be evaluated based on Eq. (7) in which is incorporated explicitly the contribution of RC frame to the shear resistance of masonry panel.
- Further, based on experimental and analytical results, the force that initiates cracking of masonry panel is approximately the same as the shear resistance of the masonry panel in an infilled RC frame.
- By comparing the force–displacement relationships of specimen 15, which contained a small split in the masonry infill, with those of Model A containing a complete split, it can be concluded that the relationship between force and displacement behaviours are approximately the same once the shear resistance of a partially continuous masonry infill has been diminished by displacement damage; in fact, the difference between the load–displacement curves for infilled and bare frames

provides the shear resistance of the masonry panel in the infilled RC frame at any displacement, as shown in Fig. 14.

- The method used to evaluate the shear resistance of the masonry panel in an infilled RC frame cannot be used for other masonry units, infill materials, strengthened masonry infill, or larger height-to-width ratios without additional research.

The results of this study substantially contribute to the state of knowledge regarding the shear strength characteristics of masonry-infilled RC frames. This research is of particular interest because it provides an enhanced empirical understanding of shear resistance theory. Further, we believe that by quantifying the shear resistance contribution of the masonry panel in an infilled RC frame, any structure built with this system can be designed more efficiently and reliably.

Acknowledgements This experimental investigation was conducted as part of the Ph.D. thesis of the first author. These tests were conducted at the Laboratory of Structural Materials Testing of the University of “Hasan Prishtina”, Kosovo. The authors are grateful to N. Kabashi for his contribution in supervising the experimental tests.

Funding This research did not receive any specific grant from funding agencies in the public, commercial, or not-for-profit sectors. Instead, this research was self-funded by the first author.

Compliance with ethical standards

Conflict of interest The authors declare that they have no conflict of interest.

Open Access This article is distributed under the terms of the Creative Commons Attribution 4.0 International License (<http://creativecommons.org/licenses/by/4.0/>), which permits unrestricted use, distribution, and reproduction in any medium, provided you give appropriate credit to the original author(s) and the source, provide a link to the Creative Commons license, and indicate if changes were made.

References

- Cascardi A, Micelli F, Aiello MA (2016) Analytical model based on artificial neural network for masonry shear walls strengthened with FRM systems. *Compos B* 95:252–263
- CEN Eurocode 6 (2004) Design of masonry structures, Part 1–1: common rules for reinforced and unreinforced masonry structures. EN 1996-1-1. European Committee for Standardisation, Brussels, Belgium
- CEN Eurocode 8 (2004) Design of structures for earthquake resistance, Part 1: general rules, seismic actions and rules for buildings. EN 1998-1. ECS, Brussels, Belgium
- Comite Euro-International Du Beton (1994) Behaviour and analysis of reinforced concrete structures under alternate actions inducing inelastic response, CEB Bulletin No.220

- Crisafuli FJ (1997) Seismic Behaviour of reinforced concrete structures with masonry infills. Ph.D. Thesis, Department of Civil Engineering, University of Canterbury
- Dautaj AD, Kabashi N (2019) Proposed analysis model for infilled reinforced concrete frames. *Proceedings of the Institution of Civil Engineers – Structures and Buildings*; 172(2): 99–112, <https://doi.org/10.1680/jstbu.17.00155>
- Dautaj AD, Kadiri Q, Kabashi N (2018) Experimental study on the contribution of masonry infill in the behavior of RC frame under seismic loading. *Eng Struct* 165:27–37
- EN 1015-11 (2007) Methods of test for mortar for masonry—Part 11: determination of flexural and compressive strength of hardened mortars, Brussels
- EN 1052-3 (2007) Methods of test for masonry—Part 3: determination of initial shear strength, Brussels
- EN 12390-3 (2002) Testing hardened concrete—Part 3: compressive strength of test specimens. Brussels
- EN 12190 (2000) Products and systems for the protection and repair of concrete structures—test methods—determination of compressive strength of repair mortar
- EN 772-1 (2011) Methods of test for masonry units. Determination of compressive strength
- Foti D, Lerna M, Vacca V (2018) Experimental characterization of traditional mortars and polyurethane foams in masonry wall. *Adv Mater Sci Eng*. <https://doi.org/10.1155/2018/8640351> (Article ID 8640351)
- Mohammad Noh N, Liberatore L, Mollaioli F, Tesfamariam S (2017) Modelling of masonry infilled RC frames subjected to cyclic loads: state of art review and modelling with OpenSees. *Eng Struct* 150:599–621
- Morandi P, Hak S, Magenes G (2018) Performance-based interpretation of in-plane cyclic tests on RC frames with strong masonry infills. *Eng Struct* 156:503–521
- Morton J (2012) Designers’ guide to Eurocode 6: design of masonry structures, EN 1996-1- 1. ICE Publishing
- Ozsayin B, Yilmaz E, Hasan Ozkaynak H, Ercan Yuksel E, Ilki A (2011) Characteristics of CFRP retrofitted hollow brick infill walls of reinforced concrete frames. *Constr Build Mater* 25:4017–4024
- Paulay T, Priestly MJN (1992) Seismic design of reinforced concrete and masonry structures. Wiley, Hoboken, New Jersey
- Penava D, Sigmund V, Kožar I, Anić F, Trajber D, Vig M (2016) Clay block masonry and mortar joint interlocking. *Grđevinar* 68(8):609–616. <https://doi.org/10.14256/JCE.1576>
- Rahman MA, Anad SC (1994) Empirical Mohr–Coulomb failure criterion for concrete block-mortar joints. *Proc Am Soc Civ Eng J Struct Eng* 120(8):2408–2422
- Razzaghi MS, Javidnia M (2015) Evaluation of the effect of infill walls on seismic performance of RC dual frames. *Int J Adv Struct Eng* 7:49–54
- Smith SB, Carter C (1969) A method of analysis for infilled frames. *Proc Inst Civ Eng* 44:31–48
- Sorić Z (2000) Mechanical properties of nonreinforced masonry walls. *Grđevinar* 52(2):67–78
- Tomazevic M (1999) Earthquake-resistant design of masonry buildings. Imperial College Press, Covent Garden, United Kingdom

Publisher’s Note Springer Nature remains neutral with regard to jurisdictional claims in published maps and institutional affiliations.

